J Mater Sci (2010) 45:4494–4500
DOI 10.1007/s10853-010-4540-2

An analysis to plastic deformation behavior of AZ31 alloys during accumulative roll bonding process

Ali A. Roostaei · A. Zarei-Hanzaki · M. H. Parsa · S. M. Fatemi-Varzaneh

Received: 23 January 2010 / Accepted: 19 April 2010 / Published online: 29 April 2010

Abstract In present investigation, the plastic deformation behavior of an AZ31 alloy during accumulative roll bonding (ARB) process was analyzed by the rigid-plastic finite element method (FEM). The finite element simulations were performed relying on the true stress–true strain behavior of the experimental alloy obtained through hot-compression testing. The equivalent plastic strain and shear strain were predicted throughout the sheet thickness. Moreover, the influence of the friction between roller/sheet and sheet/sheet on the strain distribution was analyzed. The effect of temperature on the equivalent plastic strain was also characterized. The results indicated that any increase in friction coefficient ended to an increase in equivalent plastic strain and strain gradient. Furthermore, it was found that as the temperature increased the accumulated strain decreased. This was resulted in more homogeneous deformation throughout the sheet thickness.

Introduction

As is well known the severe plastic deformation (SPD) is a promising method to facilitate manufacturing the bulky materials with sub-micrometer grain sizes. Among the diverse SPD processes, accumulative roll bonding (ARB) [1] is known as the only applicable one for continuous production of bulky materials. The key role of ARB to produce ultrafine grained materials results from the redundant shear strain introduced in the surface regions of the work piece due to the high friction condition of roller/specimen interface [2]. Therefore, understanding the strain distribution pattern and its correlation with the grain refinement of the structure plays a vital role in optimizing process parameters and enhancing the mechanical properties of the final products. Some experimental research has been previously conducted to evaluate the accumulated strains in ARB process [2, 3]. Kamikawa et al. [3] applied the embedded pin method to measure the through thickness shear strains of the ARBed sheets. Their results showed that the degree of grain refinement conform to the shear strain level. However, due to the presence of reversed shear after the neutral point [4, 5], it is believed that the embedded pin method may not properly assist calculating the shear strains.

The measurement of strain distribution in SPD techniques through experimental methods would inevitably be accompanied by some errors [3]. Accordingly, the use of a numerical method is essential in order to determine the precise strain distribution. In a recent work by Inoue and Tsuji [6], the calculated strain distribution in Al-1100 sheets processed by rolling (it was considered to follow the same conditions as ARB) has been discussed based on finite element simulation. According to their report, shear strain increased with increasing friction coefficient of roller/sheet interface. They also showed that a much larger equivalent strain (ε_{eq}) was introduced at the surface layer of the rolled sheets. This was rationalized relying on the change in the direction of the shear stress in the roll stand to opposite directions before and after a neutral plane.

The present study aims to investigate the induced plastic strain during ARB processing of AZ31 sheets using finite element analysis (FEA) [7]. Furthermore, for the purpose of meticulous inspection of governing parameters, the effects of temperature and friction between roller/sheet and

A. A. Roostaei (✉) · A. Zarei-Hanzaki · M. H. Parsa · S. M. Fatemi-Varzaneh
School of Metallurgy and Materials Engineering, University of Tehran, Tehran, Iran
e-mail: ali.roostaei@ymail.com

sheet/sheet on the through thickness deformation distributions were discussed. Moreover, the results of applied rigid-plastic FE simulation of rolling process in the same conditions as the ARB were compared in terms of shear strain distribution.

Numerical and experimental procedure

The numerical procedure of the current study was carried out applying a two-dimensional dynamic explicit finite element analysis through an explicit FE code (ABAQUS/Explicit version 6.9-1). For the sake of simplicity, the rollers were considered to be rigid bodies but the stacked sheets were regarded as two-dimensional deformable bodies. A 4 node linear plane strain thermally coupled elements were used for the sheets. Adaptive meshing was utilized in order to prevent mesh degeneration. The FEM model which was employed in this study is illustrated in Fig. 1.

The experimental material was an AZ31 magnesium alloy in the form of sheets. This was presumed to be an elastic–plastic material with a Young's modulus of 45 GPa and Poisson's ratio of 0.35 at 300 °C. Considering the predominant deformation mode in ARB (or any other rolling processes) the stress–strain relationships employed in this analysis were extracted from hot compression testing curves instead of tension curves. The hot compression tests carried out at different temperatures and constant strain rate by present author elsewhere [8], were utilized for gathering stress–strain data. These curves are depicted in Fig. 2.

Friction plays a vital role in rolling process, as it is the only mechanism by which the sheet is pulled through the roll stand. In addition, deformation profile in the rolled sheets may strongly be affected by frictional conditions [9, 10]. In this analysis, the frictional conditions at the rollers and the sheet interfaces were described by Coulomb friction model. Different friction coefficients ranging from 0.25 to 0.4 were adapted to the contacting interfaces.

The simulation was carried out for temperatures ranging from 250 to 450 °C. The heat generation due to the friction and plastic strain as well as the heat transfer to the

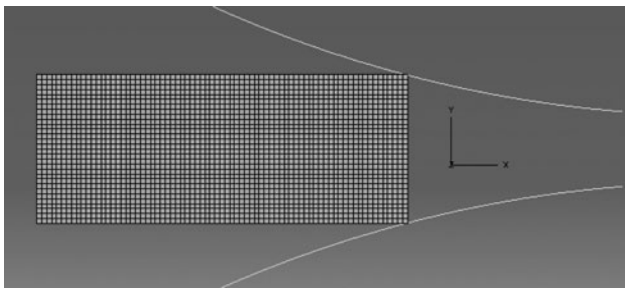

Fig. 1 The two-dimensional FEM model of ARB process

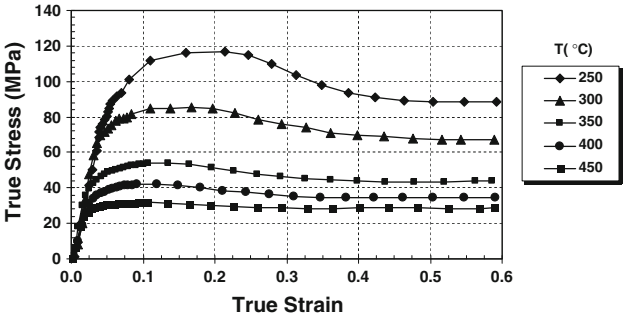

Fig. 2 The true stress–true strain curves of the experimental material at different temperatures and constant strain rate of 0.1 s^{-1}

Table 1 The computational conditions in applied finite element simulation

Density (kg/m^3)	1780
Sheet temperature (°C)	250, 300, 350, 400
Environment temperature (°C)	25
Sheet dimensions (mm)	15 × 3
Rolling reduction (%)	50
Convection coefficient (W/m^2 K)	40
Friction coefficient	0.25, 0.3, 0.35, 0.4
Thermal conductivity at 250 °C (W/m K)	101.8

environment was taken into account. The plastic strain gives rise to a heat flux per unit volume of

$$r^{\mathrm{pl}} = \eta\sigma{:}\varepsilon^{\circ\mathrm{pl}},$$

where r^{pl} is the heat flux that is added into the thermal balance, η is the inelastic heat fraction, σ is the stress, and $\varepsilon^{\circ\mathrm{pl}}$ is the rate of plastic straining [11]. The amount of inelastic heat fraction (the fraction of inelastic dissipation rate that appears as a heat flux per unit volume) which has been used in this analysis was 0.9. There is also some heat generated due to the dissipation of energy created by mechanical interaction of contacting surfaces. The fraction of this type of dissipated energy converted into heat was considered to be 1.0 and it was specified to distribute equally between the interacting surfaces. The rollers were heated to the processing temperature and therefore no heat transfer due to conduction between roller's surface and sheets were considered. Strain-rate independency for used material was hypothesized. The input parameters in finite element simulation were listed in Table 1.

Results and discussion

The optimized mesh size and deformation pattern

As is well understood the magnitude and distribution of calculated strain by FEA depends on mesh size. In fact,

decreasing the mesh size (i.e., increasing mesh density) may increase the accuracy and the time of analysis. However, there is an optimal mesh size lower than which the accuracy of calculated parameter may not significantly be changed by it. In the present research, the simulation was conducted over a range of mesh sizes in order to choose the optimized one. The accuracy of obtained results in terms of equivalent plastic strain (ε_{eq}) at the sheet surface for a given condition is shown in Fig. 3. The ε_{eq} increases with decreasing mesh size and reaches to a plateau at mesh size of 0.18 mm. The theoretical ε_{eq} in ARB process [1] was also presented.

In a quasi-static analysis, it is advantageous to reduce the computational cost by either speeding up the simulation or by scaling the material mass. In either case the value of the kinetic energy should not exceed a small fraction of the value of the strain energy. In this analysis, by monitoring kinetic energy it was made certain that the ratio of kinetic energy to internal energy does not get too large.

The predicted square grids distortion of the lower sheet through single pass ARB process with 50% reduction in thickness is presented in Fig. 4. A high degree of shear distortion occurred in the sheet surface. This has also been observed experimentally by Kamikawa et al. [3] using embedded pin.

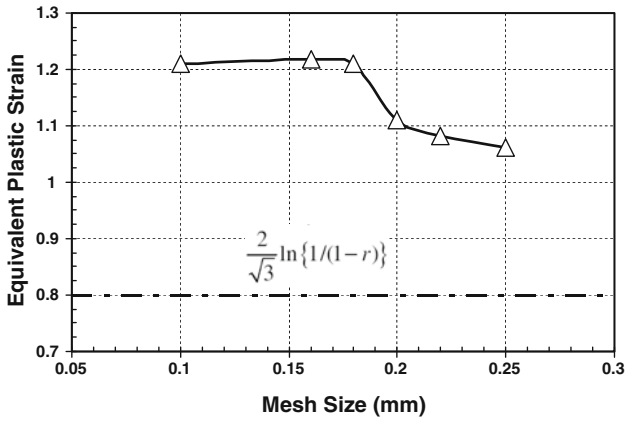

Fig. 3 The variation of ε_{eq} at surface with mesh size through thickness direction

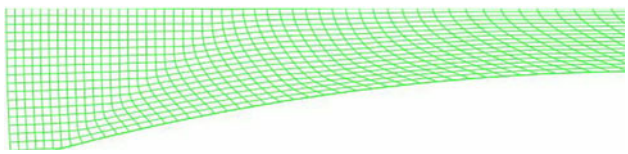

Fig. 4 The grid distortions at the lower sheet during ARB with 50% reduction

Shear strain distribution

Figure 5 shows the variation of calculated shear strain with distance from surface through the thickness for single pass ARB at 300 °C with $\mu = 0.3$. The shear strain increases monotonously from the center to the surface of the sheet. The shear component of induced strain as well as the changes in deformation mode has been considered to be the main reasons for grain refinement in ARB process [2, 12–14]. The latter may be verified through microstructural observations (Fig. 6). As is observed the surface layer with higher amount of shear strain exhibits the finer grain sizes. Using image analyzer software the mean grain sizes at the surface and center layers of the sheet thickness were measured to be 6.63 and 20.79 μm, respectively.

For better understanding, the distribution of shear strain in conventional rolling (CR) process was also analyzed to compare the results with those of ARB. The latter was also superimposed in Fig. 5. As is seen at a given condition, the magnitude of induced shear strain in single pass ARB process is greater than that of rolling process. Surprisingly, it seems that the shear strain distribution is significantly affected by the presence of interface layers. Thus, it is to conclude that not only strain accumulation due to the

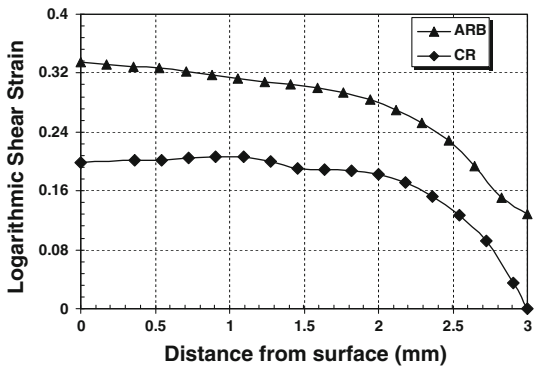

Fig. 5 The distributions of shear strain through sheet thickness for various processing routes

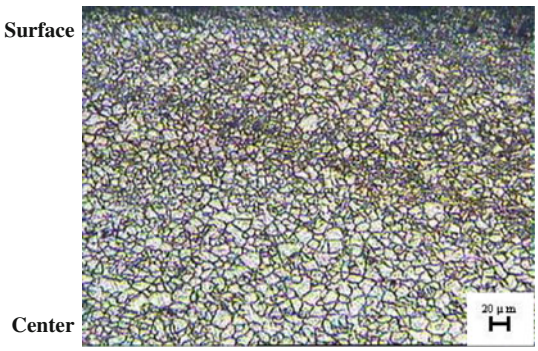

Fig. 6 The optical microstructure of ARB processed AZ31 alloy

repeatability of the process but also the presence of interface may lead the ARB process to be more effective in grain refining than conventional rolling. This may also be attributed to the higher degree of deformation constraint in ARB process. As was already reported, a significant grain refinement had been obtained through applying even a single pass ARB treatment [15].

The variation of shear strain with the friction coefficient of sheet/sheet interface is illustrated in Fig. 7. The results suggest that the amount of friction in the range of present study may not significantly affect the strain distribution.

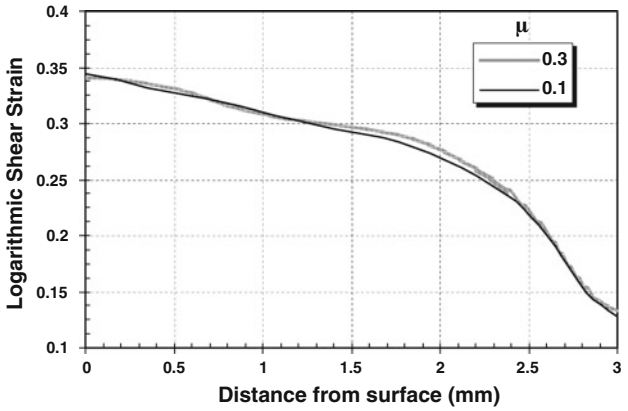

Fig. 7 The variation of shear strain through thickness with different friction coefficient at the interface

The effect of roller/sheet friction coefficient

The friction between the rollers and sheet surfaces is the only mechanism by which the sheets are drawn into the roll stand. The minimum friction coefficient necessary for successful entry is given by $\mu = \tan\alpha$, where α is the bite angle [4]. Hence, assuming $\alpha \sim 14°$ in this study, the minimum friction coefficient to fulfill this condition is about 0.25. Moreover, the friction coefficient can effectively influence the strain localization near the surface during the sheet entrance. The contours of equivalent plastic strain are depicted in Fig. 8.

The variation of calculated ε_{eq} with the distance from the surface at 300 °C for different friction coefficient of roller/sheet interface is plotted in Fig. 9. As is shown, for any certain distance the ε_{eq} increases with increasing the friction coefficient. The difference is minor at the center region and it becomes more pronounced as it approaches to the surface. An analogous friction effect has been reported for the ECAP simulation with different friction conditions [16]. In addition, the strain gradient across the thickness shows an increase with increasing friction coefficient. The strain gradient may cause a strong influence on grain

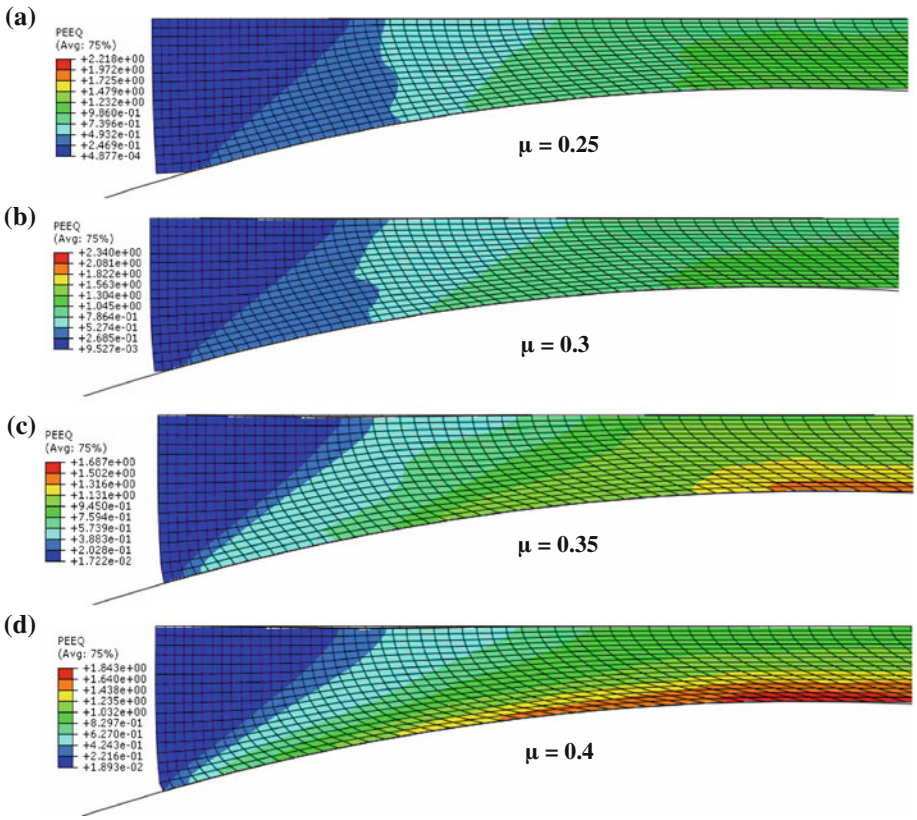

Fig. 8 The equivalent plastic strain contours obtained at 300 °C for different roller/sheet friction coefficient

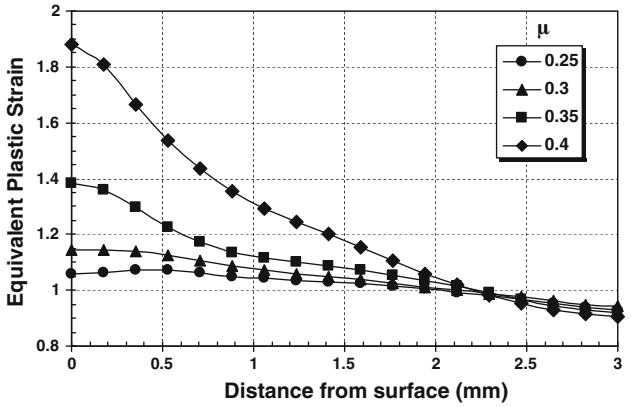

Fig. 9 The variations of ε_{eq} with sheet thickness for different roller/sheet friction coefficient

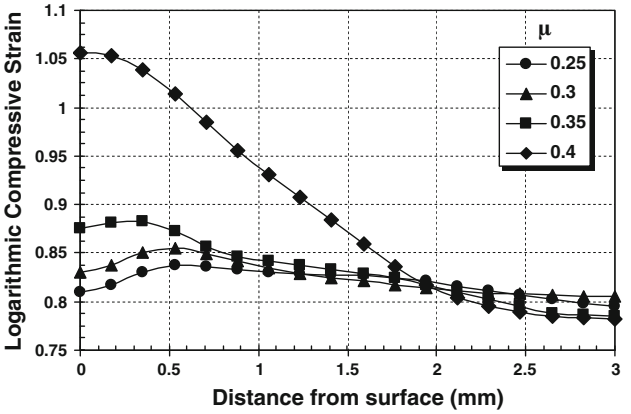

Fig. 11 The variations of compressive strain with sheet thickness for different roller/sheet friction coefficients

refinement thereby affecting the mechanical properties of the material [17].

The variation of shear strains with the distance from the surface at 300 °C for different friction coefficient of roller/sheet interface is plotted in Fig. 10. As is seen for any definite distance the induced shear strain increases with friction coefficient. This is consistent with the experimental results [3], where the shear strain is larger in a sheet rolled without lubrication than that of with it. It was found through performing a series of simulations that the shear region extended as the interface friction increased. This is resulted from the coulomb stress effects imposed by compressive stress.

As is seen in Fig. 10 the trend of shear strain variation through thickness for $\mu = 0.4$ is somewhat different from the other curves. In the other words, increasing the friction coefficient to 0.4 would alter the shear pattern throughout the thickness. This is characterized by a sharper strain gradient (shear inhomogeniety) throughout the thickness, including shear strain localization at the sheet surface. Comparing the case of $\mu = 0.4$ with the others indicates that the resulted shear strain at the thickness of 0.7 mm from the surface surprisingly falls to a lower level; whereas the ε_{eq} for this region remains topmost. Therefore, assuming that the deformation in ARB is consisted of shear deformation and plane strain compression [2], it may be concluded that the compressive strain contribution to the ε_{eq} would be greater in the case of $\mu = 0.4$. The latter is confirmed by a deeper observation in Fig. 11, where the compressive strain changes with friction coefficient in the same manner as is observed for ε_{eq}.

The effect of temperature

The variations of ε_{eq} with distance from the surface at different temperatures of 250, 300, 350, and 400 °C are presented in Fig. 12. As the temperature increases, the ε_{eq} decreases. This may lead to the finer microstructures at lower temperatures as illustrated in Fig. 13. In addition, according to Fig. 12, the strain inhomogeneity (gradient) decreases with increasing the temperature. The latter may

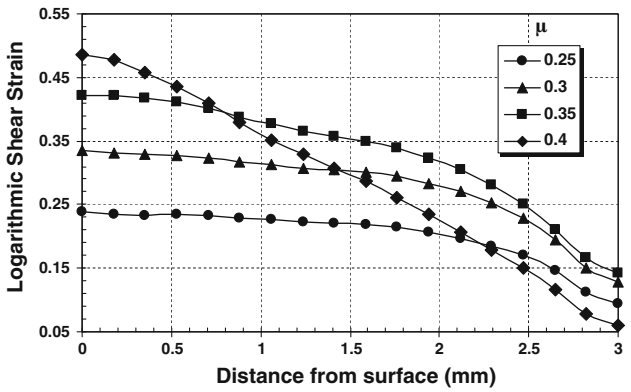

Fig. 10 The variations of shear strain with sheet thickness for different roller/sheet friction coefficient

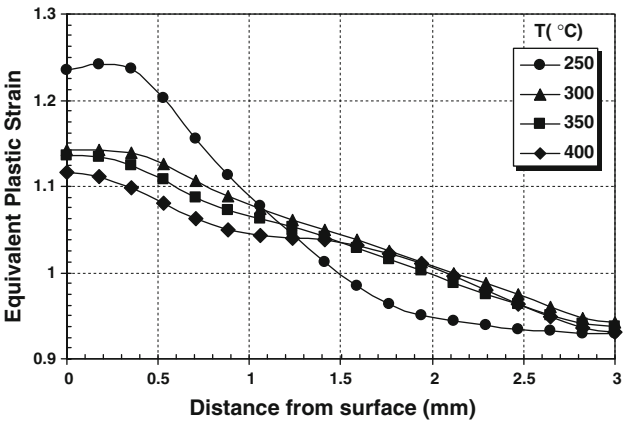

Fig. 12 The variations of ε_{eq} with distance from the surface at different processing temperatures

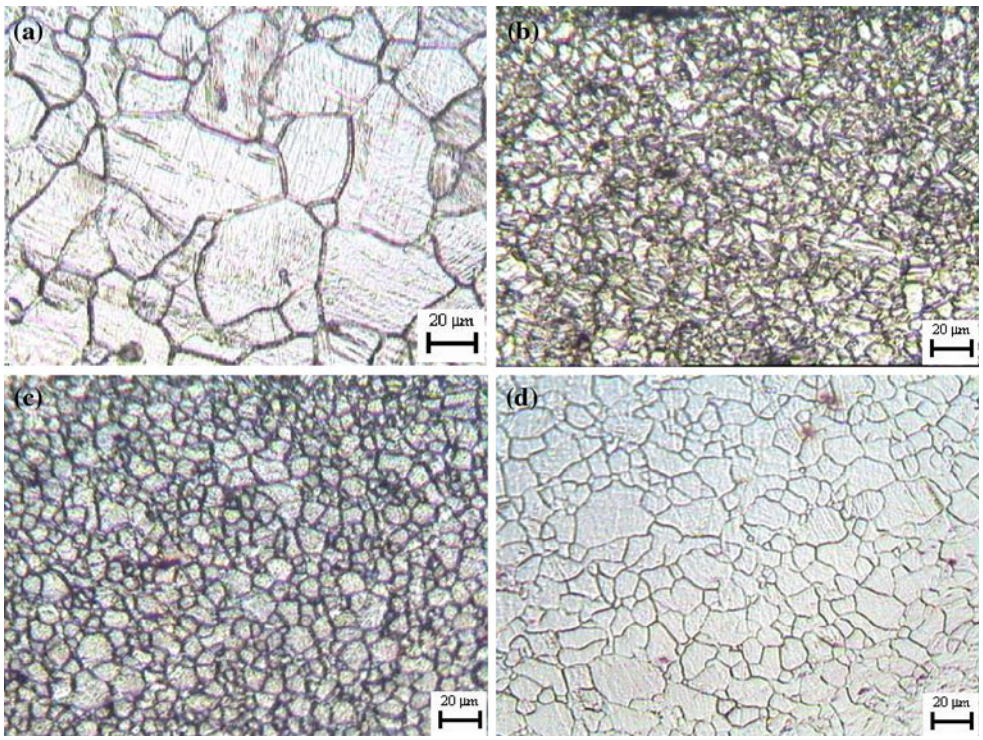

Fig. 13 The optical microstructures of ARB processed AZ31 sheets at the surface, **a** as-received, **b** 350 °C, **c** 400 °C and **d** 450 °C

be rationalized considering the facilitated flow at higher temperatures, where less constraint in material flow thereby lower amount of shear strain is anticipated for sheet layers. It is also to point out that by increasing the temperature from 250 to 300 °C, the highest strain homogeneity is achieved and above this temperature it does not vary considerably. Thus, considering the effects of grain growth and higher rate of diffusion at temperatures up to 300 °C in ARB of Mg alloys [18], this may be proposed as the optimum processing temperature for the sake of grain refining.

Conclusions

Accumulative roll bonding process was analyzed by the rigid-plastic finite element method and the results of the analyses were discussed in terms of the influence of friction conditions and processing temperature on the strain distribution through the sheet thickness. The major conclusions of this study are summarized as follows:

1. Not only the strain accumulation due to the reiteration of the process but also the presence of interface may lead the ARB process to be more effective in grain refining than conventional rolling.
2. The equivalent plastic strain increases with increasing friction coefficient. This increase is minor in the center region and it becomes more pronounced as it approaches to the surface. The compressive strain varies with friction coefficient in the same manner as is seen for ε_{eq}.
3. As the temperature increases the ε_{eq} decreases. The strain gradient also declines with increasing the processing temperature.
4. In the range of present experiments, the temperature of 300 °C and friction coefficient of 0.35 are compromised ARB processing parameters to achieve homogeneous strain distribution accompanied by no significant grain growth.

References

1. Saito Y, Utsunomiya H, Tsuji N, Sakai T (1999) Acta Mater 47:579
2. Lee SH, Saito Y, Tsuji N, Utsunomiya H, Sakai T (2002) Scripta Mater 46:281
3. Kamikawa N, Sakai T, Tsuji N (2007) Acta Mater 55:5873
4. Lenard JG (2007) Primer on flat rolling. Elsevier, London
5. Ginzburg VB, Ballas R (2000) Flat rolling fundamentals. CRC Press, Boca Raton, FL
6. Inoue T, Tsuji N (2009) Comput Mater Sci 46:261
7. Kobayashi S, Oh SI, Altan T (1989) Metal forming and the finite-element method. Oxford University Press, Oxford, p 90
8. Fatemi-Varzaneh SM, Zarei-Hanzaki A, Beladi H (2007) Mater Sci Eng A 456:52
9. Gao H, Ramalingam SC, Barbara GC, Chen G (2002) J Mater Proc Tech 124:178
10. Jiang ZY, Xiong SW, Tieu AK, Jane Wang Q (2008) J Mater Proc Tech 201:85

11. Abaqus 6.9-1 (2009) Documentation
12. Li BL, Tsuji N, Kamikawa N (2006) Mater Sci Eng A 423:331
13. Huang X, Tsuji N, Hansen N, Minamino Y (2003) Mater Sci Eng A 340:265
14. Costa ALM, Reis ACC, Kestens L, Andrade MS (2005) Mater Sci Eng A 406:279
15. Fatemi-Varzaneh SM, Zarei-Hanzaki A, Haghshenas M (2008) Int J Mod Phys B 22(18 & 19):2833
16. Suo T, Li Y, Guo Y, Liu Y (2006) Mater Sci Eng A 432:269
17. Todaka Y, Umemoto M, Yin J, Liu Z, Tsuchiya K (2007) Mater Sci Eng A 462:264
18. del Valle JA, Perez-Prado MT, Ruano OA (2005) Mater Sci Eng A 410–411:353